CrossMark

ORIGINAL PAPER

Spatiospectral Decomposition of Multi-subject EEG: Evaluating Blind Source Separation Algorithms on Real and Realistic Simulated Data

David A. Bridwell[1] · Srinivas Rachakonda[1] · Rogers F. Silva[1,2] ·
Godfrey D. Pearlson[3,4,5] · Vince D. Calhoun[1,2,3]

Abstract Electroencephalographic (EEG) oscillations predominantly appear with periods between 1 s (1 Hz) and 20 ms (50 Hz), and are subdivided into distinct frequency bands which appear to correspond to distinct cognitive processes. A variety of blind source separation (BSS) approaches have been developed and implemented within the past few decades, providing an improved isolation of these distinct processes. Within the present study, we demonstrate the feasibility of multi-subject BSS for deriving distinct EEG spatiospectral maps. Multi-subject spatiospectral EEG decompositions were implemented using the EEGIFT toolbox (http://mialab.mrn.org/software/eegift/) with real and realistic simulated datasets (the simulation code is available at http://mialab.mrn.org/software/simeeg). Twelve different decomposition algorithms were evaluated. Within the simulated data, WASOBI and COMBI appeared to be the best performing algorithms, as they decomposed the four sources across a range of component numbers and noise levels. RADICAL ICA, ERBM, INFOMAX ICA, ICA EBM, FAST ICA, and JADE OPAC decomposed a subset of sources within a smaller range of component numbers and noise levels. INFOMAX ICA, FAST ICA, WASOBI, and COMBI generated the largest number of stable sources within the real dataset and provided partially distinct views of underlying spatiospectral maps. We recommend the multi-subject BSS approach and the selected algorithms for further studies examining distinct spatiospectral networks within healthy and clinical populations.

Keywords Blind source separation · Multi-subject decomposition · Resting EEG · Simulated EEG · Wavelets · ICA

This is one of several papers published together in Brain Topography on the "Special Issue: Multisubject decomposition of EEG - methods and applications".

✉ David A. Bridwell
dbridwell@mrn.org

[1] The Mind Research Network, 1101 Yale Blvd. NE, Albuquerque, NM 87131, USA

[2] Department of ECE, University of New Mexico, Albuquerque, NM 87131, USA

[3] Department of Psychiatry, Yale University School of Medicine, New Haven, CT 06510, USA

[4] Department of Neurobiology, Yale University School of Medicine, New Haven, CT 06510, USA

[5] Olin Neuropsychiatry Research Center, Hartford Healthcare Corporation, Hartford, CT 06106, USA

Introduction

Scalp electric potentials emerge from the synchronous activity of cortical populations. These potentials are measured by electrodes on the scalp (i.e. with electroencephalography (EEG)), and are often characterized by their oscillatory properties. Scalp oscillations predominantly appear with periods between 1 s (1 Hz) and 20 ms (50 Hz), and are subdivided into distinct frequency bands which appear to correspond to distinct cognitive processes (Buzsaki 2006; Nunez and Srinivasan 2006). For example, frontal delta (1–4 Hz) and theta (4–8 Hz) responses demonstrate increased power when individuals engage in working memory and cognitive control tasks (Nyhus and Curran 2010; Harmony 2013), while occipital alpha (8–12 Hz) increases when individuals close their eyes, are drowsy, or engage in mental arithmetic (Klimesch et al. 2007). Thus, an improved characterization of these

oscillations may lead to an improved understanding of cognition within both healthy and clinical populations.

EEG reflects a mixture of cortical responses which emerge over a range of frequencies and cortical locations. A variety of blind source separation (BSS) approaches have been developed and implemented within the past few decades, providing an improved isolation of these underlying scalp sources. Temporal independent component analysis (ICA), for example, decomposes the channel × time EEG data into a linear mixture of temporally independent sources (Makeig et al. 1997; Hyvarinen et al. 2001; Stone 2004). Temporal ICA has been widely applied and demonstrates considerable utility in separating artifacts (e.g. eye movements and blinking) from EEG (Makeig et al. 2004; Onton et al. 2006) and in isolating near-dipolar scalp maps (Delorme et al. 2012). Spectral decomposition has been less widely applied, but appears well suited for separating distinct cortical sources (Hyvärinen et al. 2010).

There are a variety of approaches to spectral decomposition, with applications toward complex or real valued EEG spectra and implementations across a variety of algorithms (Anemüller et al. 2003; Bernat et al. 2005; Onton et al. 2005; Hyvärinen et al. 2010; Nikulin et al. 2011; Ramkumar et al. 2012; Shou et al. 2012; Kauppi et al. 2013; Hu et al. 2015). The majority of studies have focused on single-subject EEG decomposition, but multi-subject extensions have been increasingly developed and investigated (Kovacevic and McIntosh 2007; Congedo et al. 2010; Eichele et al. 2011; Bridwell et al. 2013; Cong et al. 2013; Lio and Boulinguez 2013; Bridwell and Calhoun 2014; Ponomarev et al. 2014; Ramkumar et al. 2014; Huster et al. 2015). There is considerable utility in further developing these multi-subject extensions, since they provide a formal approach for integrating information across subjects within a common group framework (i.e. BSS is conducted on the aggregate group matrix and the individual subject sources are derived by back reconstruction). The approach has been widely implemented for spatial decomposition of fMRI (Calhoun and Adali 2012) and may hold comparable utility for the spectral decomposition of EEG.

Within the present study, multi-subject spatiospectral EEG decompositions were implemented using the EEGIFT toolbox (Calhoun et al. 2001; Eichele et al. 2011), with real and realistic simulated datasets (the simulation code is available at http://mialab.mrn.org/software/simeeg). Decompositions were evaluated across 12 different algorithms: WASOBI, COMBI, RADICAL ICA, FBSS or ERBM, INFOMAX ICA, ICA EBM, FAST ICA, JADE OPAC, AMUSE, EVD, SIMBEC, and ERICA. These algorithms generally differ with respect to their assumptions about the underlying source distributions, whether higher order statistics are taken into account, and whether they are parametric or non-parametric (see Table 1 for references, further description, and parameter settings).

Within the present study, simulated sources were designed such that they closely resemble the frequency and spatial characteristics of real EEG. Thus, the sources are generated with biologically plausible densities and interdependence. This ensures that the algorithms are evaluated in a realistic context, and that they are robust to source characteristics which deviate from algorithmic assumptions. The findings illustrate the feasibility of decomposing multi-subject spatiospectral EEG and demonstrate which algorithms generate consistent and robust sources within real and simulated data. The spatiospectral sources are characterized by distinct spatial and spectral properties, which potentially correspond to distinct cognitive functions.

Methods (Simulated Data)

Simulating Realistic EEG with Wavelets

A wavelet-based approach was implemented to generate simulated EEG data. This approach is based upon the notion that continuous EEG may be decomposed as a convolution of a series of basis functions (i.e. wavelets) which have defined temporal and frequency properties. The distribution of the associated coefficients was estimated within select frequency bands from real data. Then, simulated wavelet coefficients were generated by randomly drawing samples from that distribution. The simulated coefficients were reconstructed within the separate frequency bands, generating simulated EEG data with temporal and spectral properties that are consistent with the EEG segment that was used to estimate the coefficient distributions.

Wavelet coefficients were estimated using the discrete wavelet transform (DWT) with biorthogonal spline mother wavelet using the *wavedec* and *wrcoef* functions in Matlab (bior3.9; dyadic decomposition; 5 levels) (http://www.mathworks.com). Detailed descriptions of the WT are provided in (Daubechies 1992; Strang and Nguyen 1996; Mallat 2009). Each level of decomposition returns two time–frequency representations with half the frequency band of the input, a course representation (i.e. the approximation A), and a high frequency representation (i.e. the detail, D). With a 250 Hz signal, the first level of decomposition returns an approximation A containing ∼0–31.25 Hz and its associated detail, D encompassing ∼31.25–62.50 Hz. At the second level, the approximation AA is ∼0–15.625 Hz and the detail AD is ∼15.625–31.25 Hz. Following this convention, we focus on the following details and approximations which approximately

Table 1 BSS algorithms evaluated in the present study

Algorithm	Citation	Description	Parameters
WASOBI	Belouchrani et al. (1997), Yeredor (2000), and Doron and Yeredor (2004); Tichavsky et al. (2006)	Reformulation of second-order blind identification (SOBI) as a weights adjusted non-linear least squares problem	Autoregressive order: 10; stabilization (rmax): 0.9
COMBI	Tichavsky et al. (2008)	Combination of efficient FAST ICA (EFICA) and WASOBI	WASOBI autoregressive order: 10; WASOBI stabilization (rmax): 0.9; EFICA epsilon: 1e-4
RADICAL ICA	Learned-Miller and Fisher (2003)	Non-parametric ICA with entropy estimates based on spacings	Angles: 150; augmented; off
FBSS or ERBM	Li and Adali (2010b)	Tradeoff between parametric and non-parametric approaches, combines EBM with a flexible correlation model	Filter length: 11
INFOMAX ICA	Bell and Sejnowski (1995)	Estimates super-gaussian sources using a fixed sigmoid nonlinearity score function	Extended: 0; sphering: on; bias: on; stop: 1e-6; max steps: 512
ICA EBM	Li and Adali (2010a)	Estimates entropy based on bounding of entropy estimates, approximates the pdf of a wide range of densities	Tolerance: 1e-4; max iterations (fastica): 100, max iterations (others): 1e3; saddle point detection: on
FAST ICA	Hyvarinen and Oja (1997), and Hyvarinen et al. (2001)	Maximizes the non-gaussianity of sources with fixed point iterations	Non-linearity: tanh; epsilon: 1e-4; max iterations: 1e3; approach: symm
JADE OPAC	Cardoso and Souloumiac (1993), and Cichocki et al. (2003)	Uses the Jacobi technique for joint approximate diagonalization of fourth order cumulants for spatial independence	
AMUSE	Tong et al. (1991)	Second order BSS, diagonalizes cross-covariance matrices	
EVD	Georgiev and Cichocki (2001)	Uses higher order correlations, does not assume non-gaussianity, non-stationarity or independence	Time delayed covariance matrices: 5
SIMBEC	Cruces et al. (2001)	Estimates sources with a contrast function based on higher order cumulants, with natural gradient ascent in a Stiefel manifold	Max iterations: 1e3; stop: 1e-; weights: [0 0 1 0 0 0]; exponents for cumulants alpha: [1 1 1 1 1 1]
ERICA	Cruces et al. (2000)	Uses a cumulant entropy cost function, achieves isotropic convergence and is independent of source distributions	Max iterations: 1e3; stop: 1e-; weights: [0 0 1 0 0 0]; exponents for cumulants alpha: [1 1 1 1 1 1]

WASOBI weights adjusted second-order blind identification, *RADICAL ICA* robust accurate direct independent components analysis, *ERBM* entropy rate bound minimization, *EBM* entropy bound minimization, *JADE* joint approximate diagonalization of eigenmatrices, *AMUSE* algorithm for multiple unknown signal extraction, *EVD* eigenvalue decomposition, *SIMBEC* simultaneous blind extraction using cumulants, *ERICA* equivariant robust independent component analysis

overlap with the characteristic EEG frequencies: delta (AAAA; ∼0–3.91 Hz), theta (AAAD; ∼3.91–7.81 Hz), alpha (AAD; ∼7.81–15.62 Hz), and beta (AD; ∼15.62–31.25 Hz).
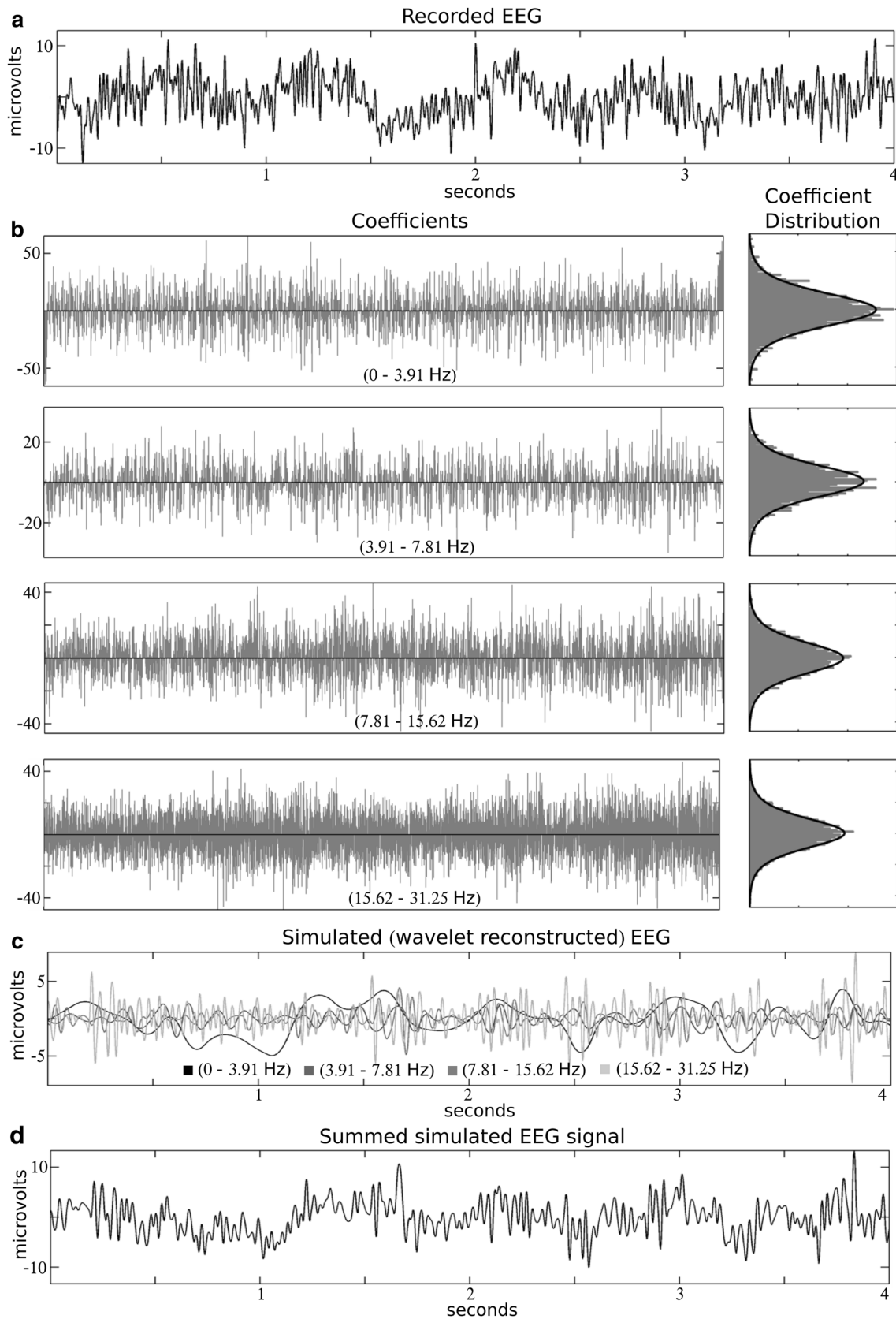
The coefficient distributions were obtained within the selected levels of decomposition (i.e. within the selected frequency bands) (Fig. 1b, right). The coefficient distributions are better approximated by a logistic distribution, with heavier tails than a Gaussian distribution. The logistic function mean and standard deviation were estimated for each of the four coefficient distributions and simulated coefficients were created by drawing values from each distribution. Simulated EEG was generated by reconstructing the simulated coefficients, generating a time course (Fig. 1c) for each of the four levels. The four levels may be summed together, generating a simulated EEG time

course with energy within the characteristic EEG frequency bands (Fig. 1d).

Simulated time courses were generated for three simulated subjects for the group spatiospectral decomposition. Within each simulated subject, wavelet coefficients were randomly drawn from the logistic distribution estimated from the original recorded EEG signal (Fig. 1a, b). Thus, we assume that the spectral characteristics are common and the time courses are uncorrelated across subjects, as expected for cortical responses collected across individuals in the absence of an explicit task (i.e. during rest).

Generating Simulated Scalp Topographies

Simulated scalp EEG topographies were generated by assigning electrode location(s) as electrical current sources

a

Recorded EEG

b

Coefficients

Coefficient
Distribution

(0 - 3.91 Hz)

(3.91 - 7.81 Hz)

(7.81 - 15.62 Hz)

(15.62 - 31.25 Hz)

c

Simulated (wavelet reconstructed) EEG

■ (0 - 3.91 Hz)   ■ (3.91 - 7.81 Hz)   ■ (7.81 - 15.62 Hz)   ■ (15.62 - 31.25 Hz)

d

Summed simulated EEG signal

◄**Fig. 1** Generating realistic simulated EEG with wavelets. A sample of real EEG (**a**) was decomposed into its time–frequency representation (**b**) with the discrete wavelet transform (DWT). The DWT filters the input by multiple matched filters that are shifted and scaled, and the coefficients (in **b**) are computed for each filter by an integral transform. The original signal can be reconstructed with an inverse wavelet transform (WT). Simulated realistic EEG may be generated by fitting the observed coefficients at each scale with a logistic distribution and generating random samples from that distribution. The simulated wavelet coefficients can then be reconstructed, generating a simulated EEG signal (in **c**) within each of the levels. These time courses may be summed together, generating a simulated time course (**d**) which resembles real EEG (**a**). Frequency-specific simulated sources were generated by separately reconstructing the simulated wavelet coefficients within each of the separate frequency bands (i.e. generating 4 time-courses (**c**) for the 4 representations (**b**)). The individual time courses were assigned a current source electrode location and a current sink electrode location (i.e. with the time series reversed in sign). The responses within the selected current source and sink electrodes were interpolated across the 60 electrode locations

and sinks, and interpolating across the neighboring electrodes. The simulated time series is assumed to represent the time series of the electrical current source, and multiplying this time series by −1 generates the time series of the electrical current sink. Simulated source 1 ($\sim$0–3.91 Hz) was assigned to electrodes Fz (current source) and Cz (sink), source 2 ($\sim$3.91–7.81 Hz) was assigned F5 and F6 (current sources) and P05 and P06 (sinks), source 3 ($\sim$7.81–15.62 Hz) was assigned P06 and F5 (current sources) and Cz (sink), and source 4 ($\sim$15.62–31.25 Hz) was assigned T7 (current source) and T8 (sink). The current sources and sinks were identical for the three simulated subjects.

The time series of neighboring electrodes was estimated by spherical interpolation using the *eeg_interp* function in EEGLAB (http://sccn.ucsd.edu/eeglab) (Delorme and Makeig 2004). Responses were generated for 60 out of 64 channels within a standard electrode layout (peripheral electrodes I1, I2, M1, and M2 were excluded in order to simplify the two dimensional topographic representations). Simulated sources were segmented (3 s epochs, 75 % overlap) and each epoch was converted to the frequency domain using a fast Fourier transform (FFT). The average spatial and spectral characteristics of the simulated sources are indicated in Fig. 2. Broadly, this approach generates a simulated scalp distribution and time series which aligns with the properties of realistic EEG, including the presence of sources and sinks and the smearing of potentials across the scalp due to volume conduction (Nunez and Srinivasan 2006).

A Few Notes on Spatiospectral BSS

There are multiple approaches to integrating EEG spectral information within a BSS framework, including approaches which operate on complex valued data (Anemüller et al. 2003; Bernat et al. 2005; Onton et al. 2005; Hyvärinen et al. 2010; Nikulin et al. 2011; Ramkumar et al. 2012; Shou et al. 2012; Kauppi et al. 2013; Hu et al. 2015). In the spatiospectral BSS implemented here (Wu et al. 2010; Bridwell et al. 2013), we focus on spectral amplitudes across channels, with the assumption that each spatiospectral map at each epoch is a mixture of spatiospectral source maps. The BSS algorithm is identical for spatiospectral BSS or temporal BSS, as it operates on a 2D matrix with repeated observations (i.e. epochs for spatiospectral BSS, and channels for temporal BSS) along the rows. The approaches differ in the manner in which the 2D matrix is constructed. Temporal BSS operates on the [channels × time] matrix of EEG voltages directly. This contrasts with spatiospectral BSS, where the (frequency × channel) information is obtained within an epoch, vectorized, and stacked across epochs, generating a 2D [epoch × (frequency × channel)] matrix of log transformed Fourier amplitudes for decomposition.

When conducting spatiospectral BSS, it is useful to consider the (frequency × channel) observation (i.e. epoch) as a map or image. Each pixel within the image has an intensity, and the location of the pixel indicates the frequency bin (row) in which the intensity was measured and its spatial location (column). This is similar to an image, where an individual pixel also describes the intensity, but locations are indicated by its position within both the column and row. In this context, spatiospectral BSS aligns closer conceptually with spatial BSS than with temporal BSS. For example, a spatiospectral EEG map within a given epoch is akin to a spatial fMRI map within a given TR. The map is a mixture of sources, and each EEG epoch, or fMRI TR, is an observation of that mixture.

It is important to consider the different mixture assumptions that underlie temporal BSS and spatiospectral BSS, as implemented here. Temporal BSS decomposes the [channels × time] matrix into a set of temporal sources and mixing matrices (i.e. topographies). These assumptions align well with the theoretical generation of EEG, where the response at a single electrode reflects the linear mixture of scalp sources (for review see Makeig et al. 2004). The linear mixture of scalp time courses might not necessarily translate to a linear mixture of the spectra of the source time courses. Thus, the assumptions of spatiospectral BSS are less tied theoretically to the generation of the underlying signals compared to temporal BSS of EEG.

Spatiospectral BSS is akin to spatial BSS of fMRI in this regard. For example, spatial independent components analysis (ICA), one of the most popular BSS approaches for fMRI, assumes that each map is a linear
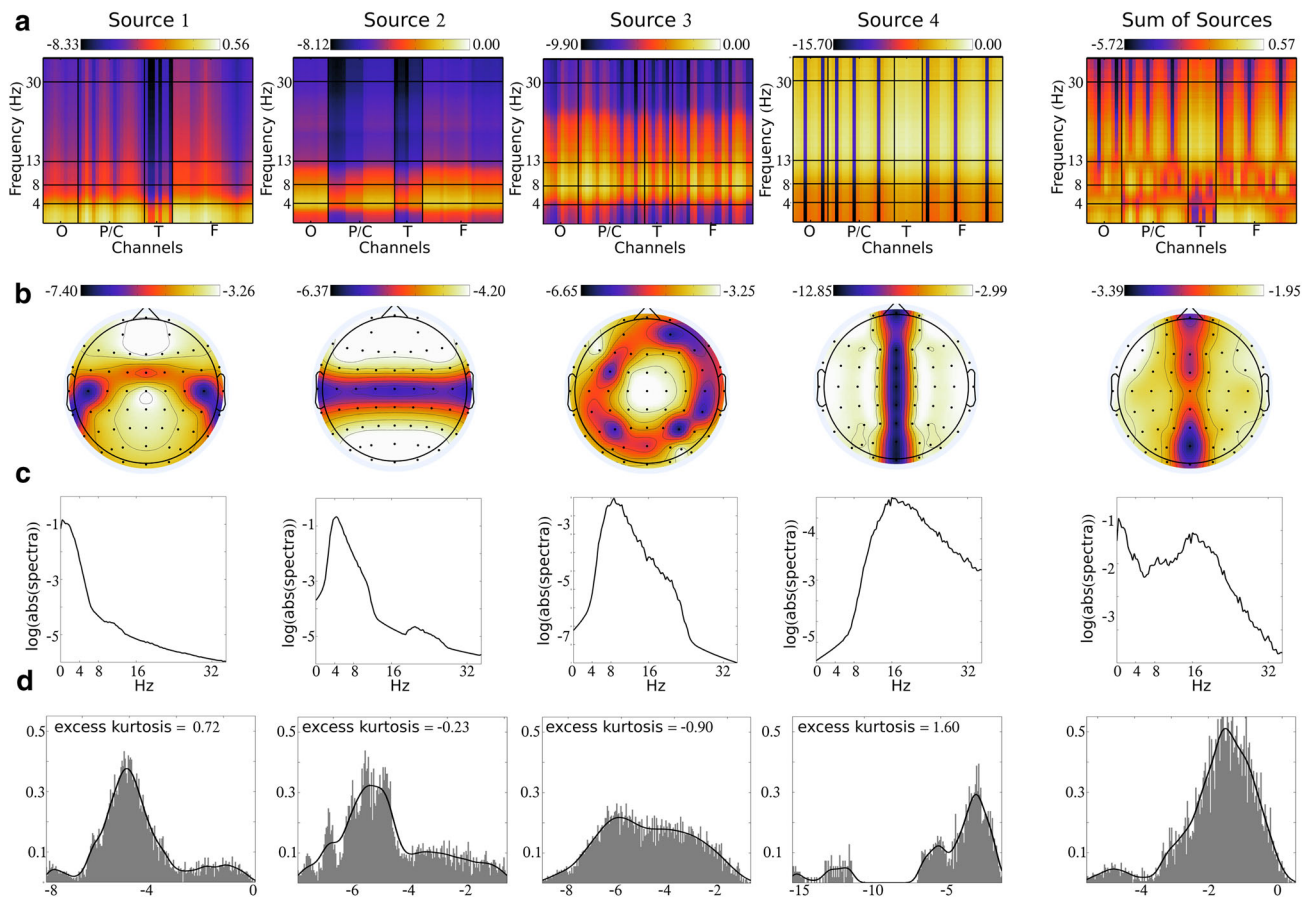
Fig. 2 Simulated spatiospectral maps. The simulated (channel × time) EEG data was segmented into 3 s epochs (75 % overlap), decomposed with the fast Fourier transform (FFT), absolute valued, and log transformed. The epochs were averaged together, generating the frequency × channel matrix in panel a. The matrix is organized (from *left* to *right*) by occipital (O), parietal/central (P/C), temporal (T), and frontal (F) electrodes (x-axis). The simulated source amplitudes (i.e. the mixing matrix) were derived from the average source map generated from an individual simulated subject (panel **a**), as described in the "Methods (Simulated Data)" section. The spatial and frequency characteristics of a single simulated subject are indicated by the log amplitude averaged across frequencies (panel **b**) and the average log amplitude across electrodes (panel **c**). Decomposition algorithms differ with respect to their assumptions about the underlying source densities. Thus, the sources (panel **a**) were vectorized, and the source distributions are indicated by the histograms in panel **d**, along with excess kurtosis (Color figure online)

mixture of statistically independent source maps, despite the highly interconnected and interdependent nature of brain networks. Nevertheless, multi-subject ICA approaches (Calhoun et al. 2001; Schmithorst and Holland 2004; Beckmann and Smith 2005; Esposito et al. 2005; Guo and Pagnoni 2008; Erhardt et al. 2011) have been usefully implemented with fMRI (for review see Calhoun and Adali 2012), and with EEG time series (Eichele et al. 2008, 2011; Bridwell et al. 2014, 2015). Spatiospectral BSS has been less widely applied within EEG, but may hold comparable utility. For example, it provides a promising approach for the multi-subject decomposition of EEG data collected in the absence of an explicit task, and generates group components with interpretable spatial and spectral characteristics (Bridwell et al. 2013).

Generating Linear Mixtures of Simulated Sources for Spatiospectral BSS

The simulated sources were segmented into 3 s epochs (750 samples per epoch) with 75 % overlap between successive epochs. The epochs were converted to the frequency domain using a FFT ($\Delta = \sim 0.33$ Hz). The complex valued Fourier coefficients were absolute valued (i.e. converted to the amplitude spectrum), log transformed, and values corresponding to 1–35 Hz were retained. These matrices were averaged across epochs separately for each simulated source, generating four spatiospectral sources (Fig. 2a) which were linearly combined within each subject, generating the source mixtures for group BSS.

In order to generate biologically plausible mixing matrices, the four simulated [channel × time] sources were

summed together, generating a single [channel × time] mixture of simulated EEG for each subject. This mixing approach aligns with the mixing assumptions of temporal BSS. In order to align with the mixing assumptions of spatiospectral BSS, the mixed [channel × time] matrix was converted into a spatiospectral [epoch × (frequency × channel)] matrix as described above. The spatiospectral sources estimated above were then linearly fit to each individual epoch, and the slope of the linear fit served as the contribution (i.e. the mixing value) for that source at that particular epoch. The final spatiospectral mixture was generated by multiplying the spatiospectral sources by the mixing matrix and summing across sources. Thus, a 379 (epochs) × 6360 (60 channels × 106 frequency bins) matrix was generated for each simulated subject, representing the linear mixture of the spatiospectral maps in Fig. 2a.

The best performing BSS algorithms will be robust to increasing noise within the observations. Thus, separate group spatiospectral decompositions were conducted with increasing noise added to the individual pixels within the [epoch × (frequency × channel)] matrix. For a particular noise level, a random sample was added to each pixel from a Gaussian distribution with zero mean and a standard deviation of 1, 5, 10, 15, or 20 % of the median of all values within the 2D data matrix.

Group Spatiospectral Decomposition

Group spatiospectral decompositions were conducted with the EEGIFT toolbox (http://mialab.mrn.org/software/eegift/) version 4.0a. The toolbox provides a formal approach for integrating the individual EEG recordings into aggregate group (frequency × channel) EEG components. Each individual dataset was reduced with PCA (20 components) and concatenated into an aggregate [20 PCA components × 3 subjects] × [106 frequencies × 60 channel] 2D matrix. The aggregate group matrix is then decomposed into an underlying source matrix and a mixing matrix (for a detailed description of the Group ICA implementation, please see Calhoun et al. 2001; Eichele et al. 2011). The approach alleviates issues with aligning sources from independent decompositions while enabling evaluation of individual subject differences via individual back-reconstructed components (Calhoun et al. 2001; Beckmann and Smith 2005; Erhardt et al. 2011).

Group spatiospectral BSS was conducted with 12 different decomposition algorithms (see Table 1). Twenty spatiospectral decompositions were conducted for each algorithm in order to evaluate decompositions with increasing levels of added noise (five levels) and with an increasing number of estimated components (5, 10, 15, and 20 estimated components). ICASSO analysis was conducted within each of the twenty decompositions in order

to ensure that the sources were stable (15 iterations; bootstrap resampling; random initializations) (Himberg et al. 2004).

Algorithm Evaluation

The algorithms were evaluated based on the stability of the source estimates and the correlation between the simulated source maps and the BSS source spatiospectral maps. Each simulated source (n = 4) was correlated with each of the BSS sources (n = 5, 10, 15, or 20) and the BSS source with the highest correlation was selected. Sources are considered highly stable across decompositions if their stability index I_q is greater or equal to 0.90.

Results (Simulated Data)

Simulating Realistic EEG

A wavelet based approach was implemented to generate realistic simulated EEG time courses. Wavelet coefficient distributions were fit to a logistic function for the four levels of decomposition which contribute to the EEG frequencies of interest. As demonstrated in Fig. 1b(right), the distribution of wavelet coefficients (indicated by the gray histogram) can be well approximated by the logistic function (indicated by the black line). Simulated coefficients were randomly drawn from this distribution and converted to the time domain. The temporal characteristics of the simulated time course (Fig. 1d) closely resemble the temporal characteristics of real EEG (Fig. 1a).

Realistic scalp topographies were generated by assigning the simulated time course to source and sink electrodes and interpolating the simulated time course response across the remaining electrodes. The average spatiospectral map was generated for each source (Fig. 2a). The topographic map in Fig. 2b indicates the sum of the spatiospectral map across frequencies, and the plots in Fig. 2c indicate the sum across electrodes. Source 1 is characterized by frontal and central/parietal responses within the delta band, source 2 is characterized by frontal and occipital responses within the theta band, source 3 is characterized by central/parietal responses within the alpha band, and source 4 is characterized by left and right temporal responses within the beta band. These images broadly demonstrate that the simulated source spectral and spatial properties align with the frequency and spatial characteristics anticipated from real EEG.

Simulated Source Distributions and Dependence

BSS algorithms can differ with respect to their assumptions about source distributions and source interdependence. The

simulated source distributions (i.e. histograms) are displayed in Fig. 1d. Sources 1 and 2 demonstrate a single peak, source 3 appears to demonstrate two broad peaks, and source 4 demonstrates multiple peaks. Excess kurtosis values range from −0.90 to 1.60, with values <0 indicating reduced concentration around the mean and values >0 indicating greater concentration around the mean (compared to a Gaussian distribution). The sources demonstrate considerable interdependence (see Fig. 3), with correlations >0.20 among sources 1 and 2 (r = 0.68), sources 1 and 3 (r = 0.21), and sources 2 and 3 (r = 0.48). Source 4 was negatively correlated with sources 1, 2, and 3 (r = −0.46, −0.33, and −0.12, respectively). These source distributions and dependencies may be less than optimal for certain BSS algorithms (e.g. INFOMAX ICA emphasizes both sparsity and statistical independence (Calhoun et al. 2013)). However, the source distributions and dependencies are biologically plausible, since the spatiospectral maps align with the spatial and spectral properties anticipated from real EEG. Thus, algorithm's which are robust to these source characteristics will likely be optimal for real EEG.

Evaluating Group Spatiospectral Decompositions

The BSS algorithm performance was evaluated by identifying the BSS source with the highest correlation with the simulated source and examining correlations across algorithms. These values are plotted in Fig. 4 for each of the 12 algorithms, 4 sources, 4 estimated component numbers, and 5 noise levels. For example, the 4 × 5 square in the upper left hand corner (corresponding to WASOBI and source 1) indicates the highest correlation between the estimated sources and source 1 across increasing noise levels (each column) and increasing component numbers (each row). The correlation is highest when the component number approaches the true number of sources (top pixels), and with decreasing noise (left pixels). The individual pixels are colored black if the selected component was unstable (i.e. if $I_q < 0.90$). The algorithms are organized with the highest overall average correlation on top and the lowest overall average correlation on bottom.

Optimal performance is indicated by the presence of bright pixels across all component and noise levels. In general, AMUSE, EVD, SIMBEC, and ERICA were

Fig. 3 Dependence among sources. Different decomposition algorithms are sensitive to different degrees of source dependence. The dependence among the simulated sources are indicated by scatterplots with the separate source values on the x and y axis. The correlations among source pairs are indicated within the upper left of each plot. In general, there is considerable dependence among the sources. Thus, the best performing algorithms within the present study should be robust to the degree of dependence observed within these realistically simulated sources
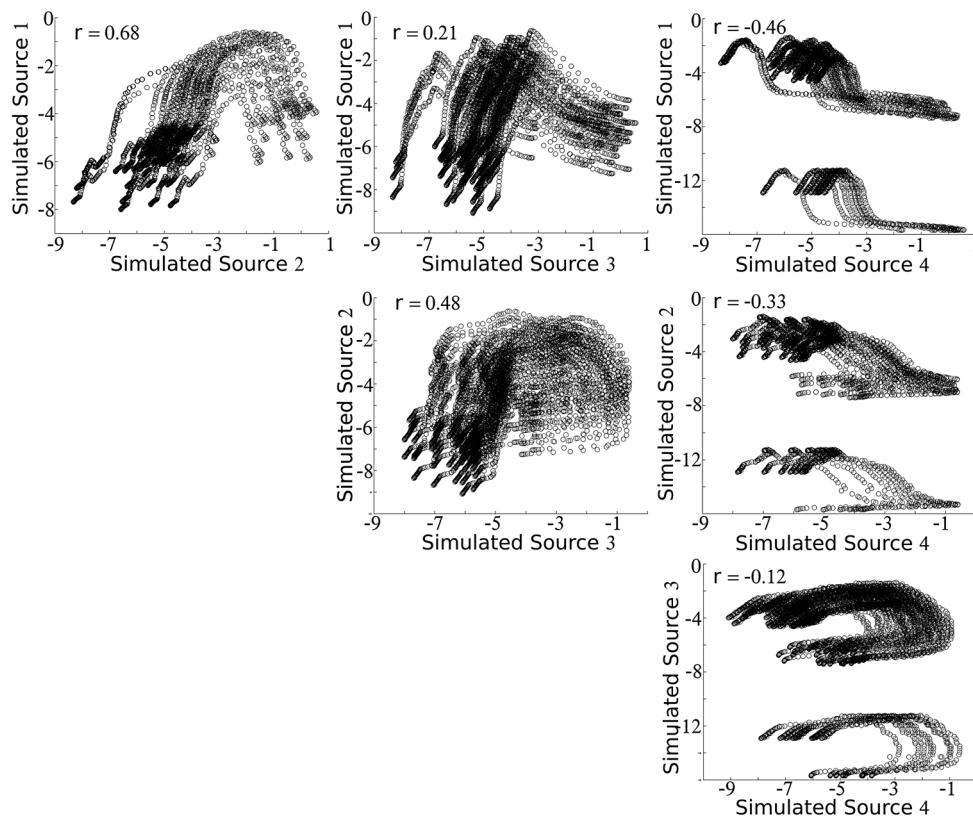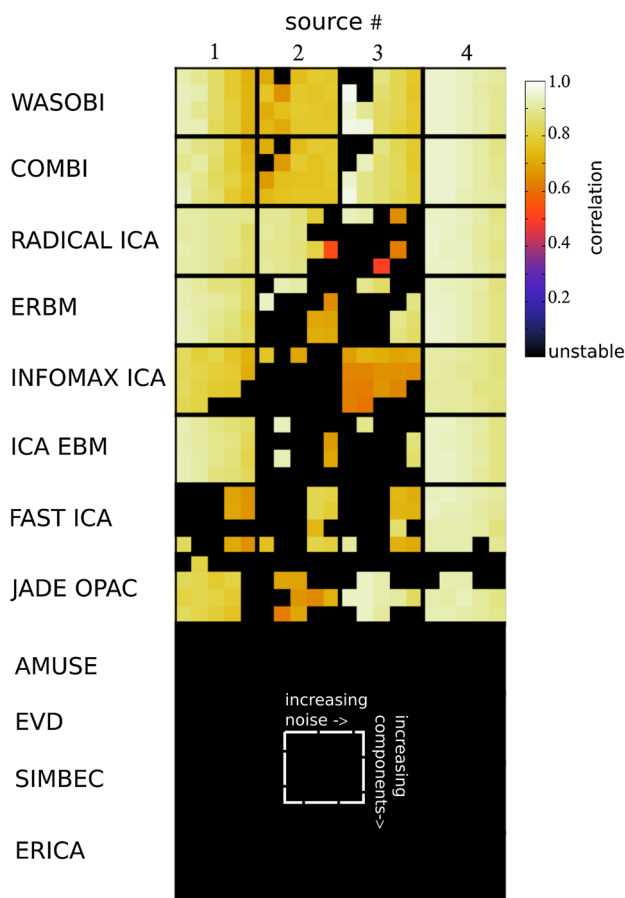
Fig. 4 Correlation between BSS sources and simulated sources. The correlations between the simulated sources and BSS sources are indicated within each *square*. Correlations are demonstrated for each algorithm (*rows*) and source number (*columns*) within a 4 × 5 block. The block is organized with increasing (from *left* to *right*) added noise (1, 5, 10, 15, and 20 %) and with an increasing (from *top* to *bottom*) number of estimated components (5, 10, 15, and 20 components). The correlation within each square is plotted along a color continuum (see colorbar) if the highest correlated source is stable across multiple ICA runs ($I_q \geq 0.90$). Unstable sources are indicated by a black square. For example, consider the *yellow square* within the *upper left hand corner*. This *square* indicates high correlation between one of the 5 sources estimated with the WASOBI algorithm, and simulated source 1, with 1 % added noise. The presence of high correlations within the remainder of the 4 × 5 block indicates that the WASOBI algorithm successfully decomposed source 1 over a range of added noise levels and estimated components (Color figure online)

unable to generate stable sources for all simulated sources, component levels, and noise levels. Source 4 was successfully decomposed with 8 out of the 12 algorithms (WASOBI, COMBI, RADICAL ICA, ERBM, INFOMAX ICA, ICA EBM, FAST ICA, and JADE OPAC). Decompositions of sources 1, 2, and 3 were more variable across the eight algorithms. In particular, sources 2 and 3 were best decomposed with WASOBI and COMBI, which suggests that these two algorithms best generalize across a range of source characteristics, noise levels, and component numbers. The

similarity between WASOBI and COMBI suggests that WASOBI primarily contributes to the improved performance of COMBI within the present study.

Methods (Real Data)

Participants

Fifty four healthy individuals participated at the Institute of Living at Hartford Hospital. The study was conducted in accordance with an experimental protocol approved by the Institutional Review Board (IRB). Participants were free from lifetime psychotic or mood disorder and a family history of psychotic or BP disorders in first-degree relatives (Family History Research Diagnostic Criteria (Andreasen et al. 1977)). Twenty four of the participants were males and 30 were females. The average age was 36.93 years (min 19; max 66; SD 12.54).

EEG Acquisition and Preprocessing

Participants were instructed to rest with their eyes open for 5 min. EEG was recorded with a 66-channel Neuroscan system (Compumedics, Charlotte, NC). Silver/silver chloride electrodes were placed according to the International 10–10 system with a mid-forehead ground and nose reference (sampling rate = 1000 Hz; impedance ≤5 kΩ). EEG preprocessing was conducted in Matlab (http://www.mathworks.com) using custom functions, built-in functions, and the EEGLAB toolbox (http://sccn.ucsd.edu/eeglab).

Approximately 4 min 47 s (287240 samples) of EEG was processed and analyzed for each subject. Peripheral electrodes I1, I2, M1, and M2 were excluded from analysis in order to simplify the two dimensional topographic representations and for consistency with the simulated data. The EEG data was linearly detrended, and forward and backward filtered with a Butterworth filter (bandpass: ~0.01–50 Hz). The data was referenced to channel Cz and bad channels were identified based on the data distribution and variance of channels, as implemented in EEGLAB's *pop_rejchan* function (Delorme and Makeig 2004) and the FASTER toolbox (Nolan et al. 2010), and spherically interpolated. An average of 1.70 channels were interpolated (min 0; max 5; SD 1.42).

The EEG data was average referenced and artifacts were attenuated by conducting a temporal ICA decomposition on the individual recordings (extended INFOMAX ICA algorithm in EEGLAB (Bell and Sejnowski 1995; Lee et al. 1999)), detecting artifactual sources with the ADJUST toolbox (Mognon et al. 2011), and reconstructing to the original data space. An average of 1.91 sources were eliminated (min 0; max 7; SD 1.89).

Consistent with the simulated data, each individual EEG recording was segmented into 3 s epochs (750 samples per epoch) with 75 % overlap between successive epochs. The epochs were converted to the frequency domain by the FFT ($\Delta = \sim 0.33$ Hz). The complex valued Fourier coefficients were absolute valued (i.e. converted to the amplitude spectrum), log transformed, and values corresponding to 1–35 Hz were retained.

BSS Model Order

The model order, i.e. the number of estimated components, is an important consideration in BSS. At the group level, the number of estimated components has previously been derived using minimum description length (MDL) criteria (Li et al. 2007). The number of stable sources may be additionally used as a guide for model order selection. For example, our simulations indicate that the maximum number of stable sources rarely exceeds the true number of underlying sources (e.g. the maximum number of stable sources was five (nine out of $4 \times 5 \times 12 = 240$ decompositions), which is one more than the true number of underlying sources). Based on these findings, we have selected a model order for real EEG decomposition such that the number of estimated sources (N = 15) is slightly larger than the maximum number of stable sources (N = 12).

Group Spatiospectral Decomposition

Group spatiospectral decompositions were conducted with the EEGIFT toolbox (http://mialab.mrn.org/software/eegift/) version 4.0a. Each individual dataset was reduced with PCA (20 components) and concatenated into an aggregate [20 PCA components × 54 subjects] × [106 frequencies × 60 channel] 2D matrix. The aggregate group matrix was then decomposed into an underlying source matrix and a mixing matrix (Calhoun et al. 2001; Eichele et al. 2011; Erhardt et al. 2011). Fifteen components were estimated for each decomposition, and ICASSO analysis was conducted within each of the decompositions in order to ensure that the sources were stable (15 iterations; bootstrap resampling; random initializations) (Himberg et al. 2004). Spatiospectral decompositions were conducted with the 12 algorithms described previously (Table 1).

Results (Real Data)

Unique Sources Among BSS Algorithms

Fifteen sources were estimated for each of the 12 decomposition algorithms. Fifty-two of the 165 estimated sources were stable $I_q \geq 0.90$, and 15 of the 52 estimated sources

were unique. These 15 spatiospectral sources are indicated in Fig. 5. The algorithms in which the source appeared are indicated by the 12 pixel grid located below each plot (white pixels indicate that the source was present and stable within that particular algorithm, the algorithms are labeled in the lower right hand corner). For example, source 10, which is characterized by a response within the alpha frequency band (i.e. between 8 and 12 Hz), was present within the decompositions with WASOBI, COMBI, INFOMAX ICA, FAST ICA, and JADE OPAC algorithms. These results are summarized across the algorithms and sources within Fig. 6. The algorithms are organized by their performance within the simulated data, with the best performing algorithm on top and the worst performing algorithms on bottom. When comparing Fig. 4 with Fig. 6, we note that the algorithms which resulted in unstable components within the simulated data also generate unstable components within the real dataset. WASOBI, COMBI, INFOMAX ICA, and FAST ICA generated 10, 10, 12, and 11 out of the 15 unique sources, respectively, with the other algorithms individually contributing 6 unique sources or less. WASOBI and COMBI appear optimal since they decomposed many of the unique sources identified within the real data and were the best performing algorithms within the simulated dataset (Fig. 4).

Source Topographies

Figure 7 illustrates the spatial characteristics of the 15 sources in Fig. 5. Topographic distributions were created within each of the 15 sources by averaging across channels, identifying the frequency band within the full width half maximum surrounding the peak, and averaging each channel within the selected frequency range. The sources generally demonstrate widespread responses with peaks often centered within occipital/parietal and frontal electrode locations. For example, sources 7, 8, 9, and 10 demonstrate peak frequencies within the alpha band (i.e. 8–12 Hz) with topographic peaks over frontal and occipital/parietal scalp locations. This pattern is consistent with the topography of alpha responses demonstrated previously, including studies implementing spatiospectral BSS's (Shou et al. 2012; Bridwell et al. 2013). In general, the spatial characteristics of the sources generated from real data appear biologically plausible, and they qualitatively resemble the spatial topographies of the simulated dataset (compare Fig. 2b with Fig. 7).

Discussion

Within the present study, we demonstrate the feasibility of decomposing multi-subject spatiospectral EEG and identify the algorithms which generate consistent and interpretable sources. For simulations, the algorithms were
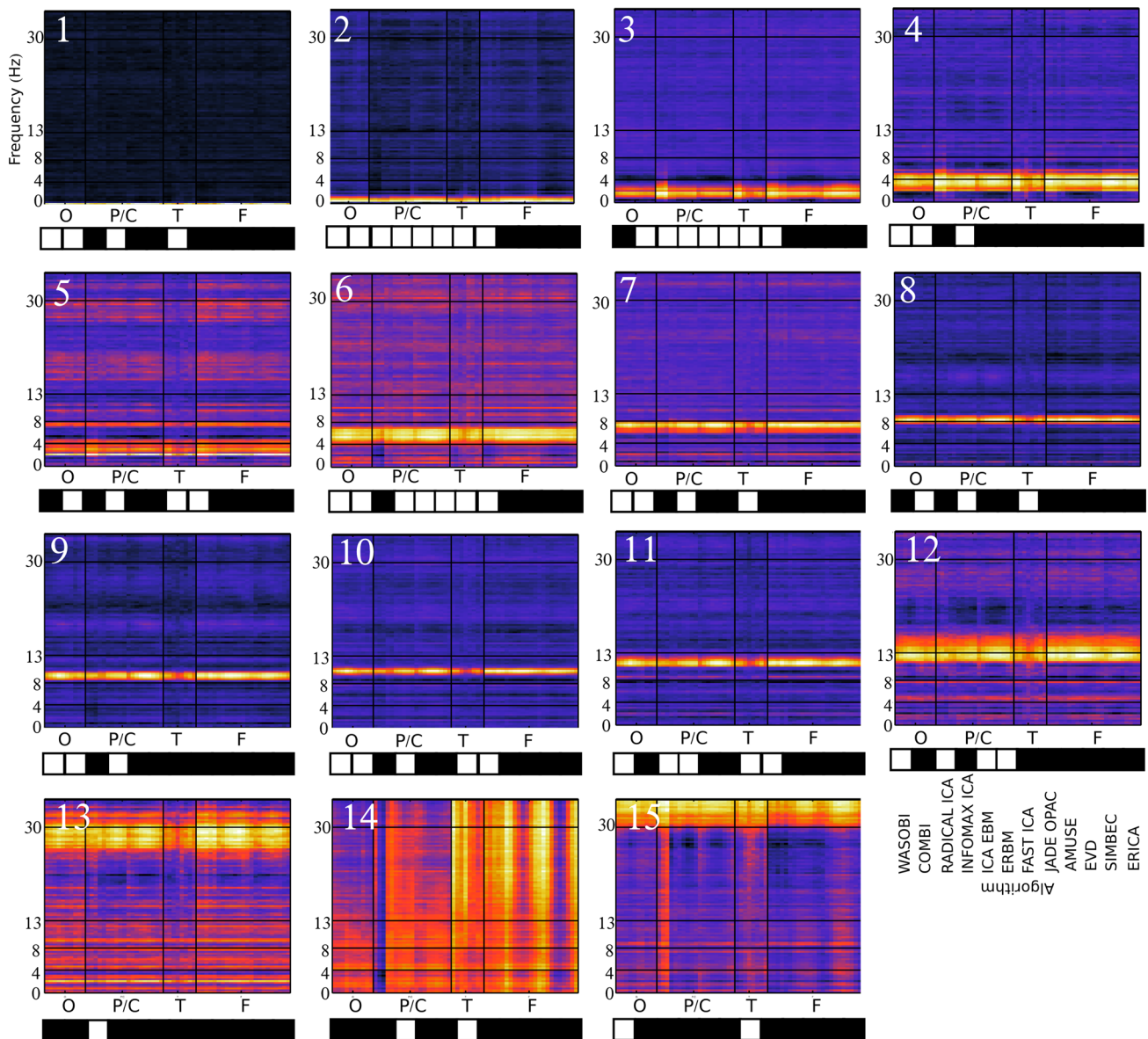
Fig. 5 Spatiospectral maps derived from real EEG. Spatiospectral BSS was conducted for each of the 12 decomposition algorithms, and 15 unique sources were identified across all algorithms. The unique sources are indicated in the frequency × channel plots above. A representative source was selected in instances where the spatiospectral map appeared across multiple decompositions. The sources are organized from low (1, *upper left*) to high (15, *lower right*) frequency. The individual plots are organized (from left to right) by occipital (O), parietal/central (P/C), temporal (T), and frontal (F) electrodes (x-axis). The maps are individually scaled so that they each encompass the full range of the colormap. The units are not indicated, since their magnitudes are not directly interpretable across different decompositions. The grid below each source indicates the algorithms which decomposed that source. A *solid white square* indicates that the source was present and stable (with $I_q \geq 0.90$), and a *solid black square* indicates that it was not present and/or not stable. The algorithms are labeled in the lower right. The algorithms are organized based on their performance within the simulated data (see Fig. 3), with the best performing algorithm on the *left*, and the worst performing algorithm on the *right*

evaluated with respect to their stability and the similarity between group sources and simulated sources. WASOBI and COMBI appeared to be the best performing algorithms, as they decomposed the four simulated sources across a range of component numbers and noise levels. RADICAL ICA, ERBM, INFOMAX ICA, ICA EBM, FAST ICA, and JADE OPAC decomposed a subset of the sources within a subset of component numbers and noise levels, while AMUSE, EVD, SIMBEC, and ERICA generated unstable sources (Fig. 4). These findings are consistent with a previous study demonstrating greater reliability of INFOMAX ICA, FAST ICA, and JADE compared to SIMBEC
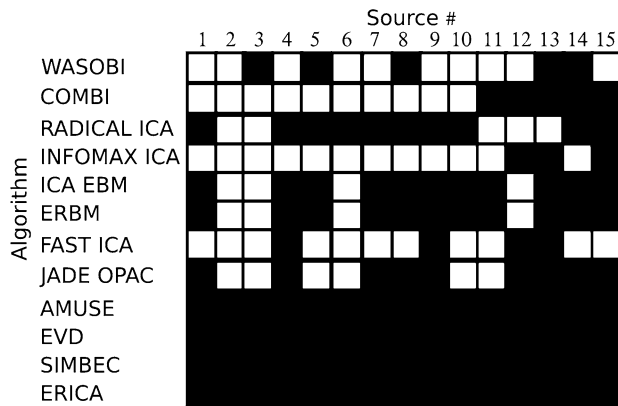
Fig. 6 Stable sources within each BSS algorithm. The grid demonstrates which sources were present and stable within each of the 12 BSS algorithms. The 15 spatiospectral sources are indicated in Fig. 5. The grid columns are also displayed under each of the sources in Fig. 5. A *solid white square* indicates that the source was present and stable (with $I_q \geq 0.90$) for the algorithm listed on the left. The algorithms are organized based on their performance within the simulated data (see Fig. 3), with the best performing algorithm on *top*, and the worst performing algorithms on *bottom*

and AMUSE for spatial fMRI group BSS (Correa et al. 2005) and add to previous studies evaluating different BSS algorithms for decomposition of EEG (Eichele et al. 2011; Delorme et al. 2012; Huster et al. 2015).

For real data, we examined the number of stable sources generated within each algorithm and identified sources which were consistent across algorithms. INFOMAX ICA, FAST ICA, WASOBI, and COMBI generated the largest number of stable sources (12, 11, 10, and 10, respectively) (Figs. 5, 6). Different algorithms demonstrate different subsets of sources, indicating that they provide partially distinct views of underlying spatiospectral maps. Thus, the algorithms are complementary, and a more comprehensive picture may emerge by integrating findings across different algorithms. For example, the full diversity of sources (i.e. the 15 unique spatiospectral maps in Fig. 5) could be obtained by integrating results from INFOMAX ICA (sources 1-11 and 14), RADICAL ICA (sources 12 and 13), and FAST ICA (source 15) (Fig. 6). Thus, the different algorithms demonstrate different strengths and weaknesses,

Fig. 7 Source topographies. Topographic distributions were generated within each of the 15 sources by averaging across channels, identifying the frequency band within the full width half maximum surrounding the peak, and averaging each channel within the selected frequency range. The maps are scaled so that they each encompass the full range of the colormap. The units are not indicated, since their magnitudes are not directly interpretable across different algorithms
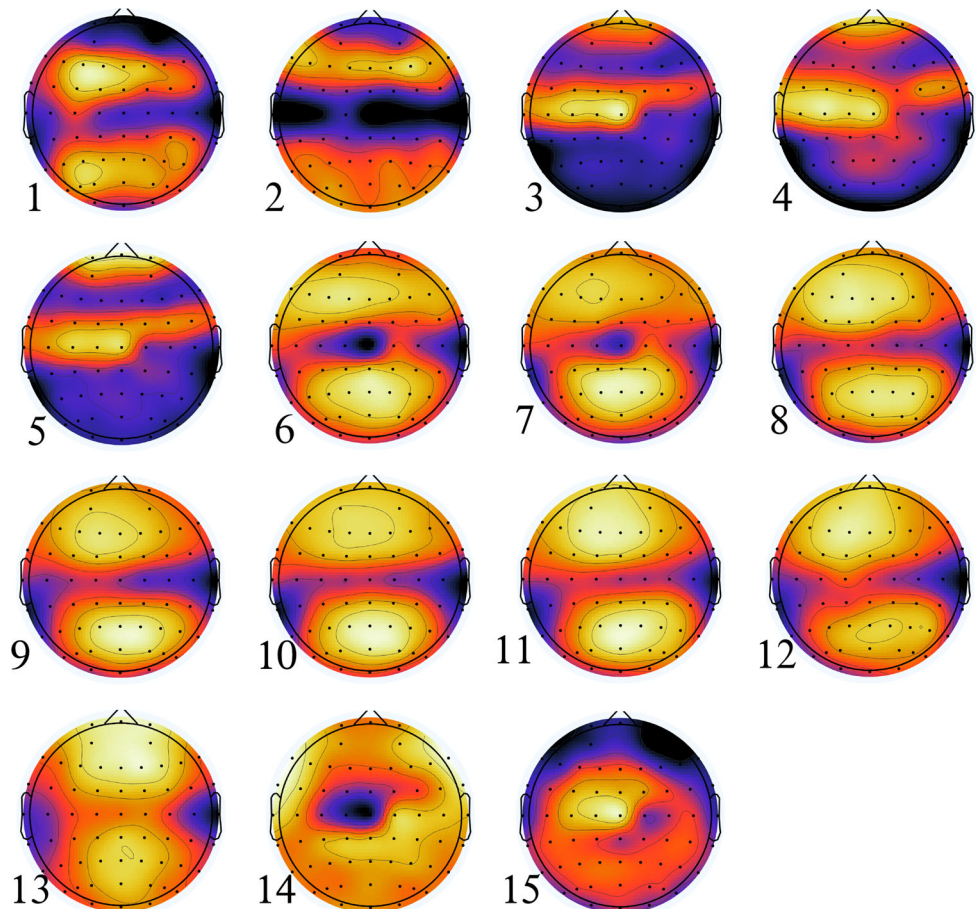
and isolate different subsets of sources. Integrating information across algorithms may overcome the limitations of any individual algorithm.

The 15 components derived from real data each demonstrate frequency and spatial properties that are characteristic of EEG. Sources 2 and 3 demonstrate a response within the delta band (1–4 Hz) which peaks over frontal and parietal/occipital electrodes (source 2), or over frontal/temporal electrodes (source 3). Interestingly, these sources were decomposed with 7 out of the 8 algorithms (COMBI, RADICAL ICA, ERBM, INFOMAX ICA, ICA EBM, FAST ICA, and JADE OPAC) which successfully decomposed a subset of sources within the simulated dataset (compare Figs. 4, 6). Source 6 demonstrates a peak response within the theta band (4–8 Hz) over frontal and parietal/occipital electrodes, while sources 8–12 demonstrate peaks within different regions of the alpha band (8–12 Hz), but with similar topographies. In general, the sources within the present study closely resemble the sources identified with group spatiospectral ICA of a separate 32 channel EEG dataset (Bridwell et al. 2013).

Temporal ICA is the most widely applied approach to EEG decomposition, but is limited with respect to its ability decompose EEG oscillations (i.e. its ability to separate signal from signal). Instead, temporal ICA is better suited to separating EEG artifact, since it has the most non-Gaussian distribution (Hyvärinen et al. 2010). A number of approaches have been developed to better emphasize distinct EEG oscillations within BSS, including second-order blind identification (SOBI) (Belouchrani et al. 1997; Tang et al. 2005; Tang 2010), approximate joint diagonalization of cospectra (AJDC) (Congedo et al. 2008), recursive multi-dimensional decomposition (R-MDD) (Orekhova et al. 2011), hierarchical Bayesian learning (Wu et al. 2011), and functional source separation (FSS) (Porcaro et al. 2010). Spectral ICA has also demonstrated considerable utility in decomposing EEG oscillations (Hyvärinen et al. 2010), consistent with the present findings.

The current group spatiospectral BSS approach discards phase information and may be implemented in instances where experimental events are not aligned across subjects, or in the absence of an explicit task (i.e. during rest). With spatiospectral BSS, differences across tasks will emerge as differences in the mixing matrix weights instead of differences within the sources (i.e. as with group temporal ICA). In the case of tasks, it's important to note that the temporal resolution depends on the choice of epoch length and overlap. For example, with a 75 % overlap and 3000 ms epoch length, weights were obtained for each source at 750 ms intervals. Increasing the overlap or reducing the epoch length would provide an improved resolution of spatiospectral maps which precede and follow a particular experimental event. These findings will help clarify the relationship between spatiospectral maps and cognitive function.

Multi-subject spatiospectral decomposition, as implemented here, implicitly assumes that spatiospectral sources are similar across subjects. Realistic data deviates from this assumption, as there is considerable variability in the topography and peak frequency of EEG responses across individuals (Klimesch 1999). Previous studies have examined the influence of inter-subject variability on group spatial fMRI ICA, and group temporal EEG ICA stimulations (Allen et al. 2012; Huster et al. 2015). Group ICA appears robust to inter-subject differences within spatial fMRI simulations, with decompositions often reflecting an optimal tradeoff between estimating a given source at the group level and preserving differences in the individual subject back-reconstructed sources (Allen et al. 2012). Group ICA of temporal EEG also appears robust to inter-subject differences in timing, with sources successfully decomposed with up to ∼200 ms of temporal jitter across subjects (Huster et al. 2015). It will be important for further studies to examine the nature and degree in which these inter-subject differences are preserved in group spatiospectral decompositions.

Summary and Conclusion

The findings demonstrate the feasibility of multi-subject BSS for deriving distinct EEG spatiospectral maps. A subset of BSS algorithms produced consistent and robust sources within real and simulated EEG datasets. Within simulations, WASOBI and COMBI appeared to be the best performing algorithms, as they decomposed the four sources across a range of component numbers and noise levels. RADICAL ICA, ERBM, INFOMAX ICA, ICA EBM, FAST ICA, and JADE OPAC decomposed a subset of the sources within a subset of component numbers and noise levels. INFOMAX ICA, FAST ICA, WASOBI, and COMBI generated the largest number of stable sources within the real dataset, and the different algorithms provided partially distinct views of underlying spatiospectral maps. The multi-subject BSS approach, and the selected algorithms, will be useful for further studies examining distinct spatiospectral networks within healthy and clinical populations.

References

Allen EA, Erhardt EB, Wei Y et al (2012) Capturing inter-subject variability with group independent component analysis of fMRI data: a simulation study. NeuroImage 59:4141–4159. doi:10.1016/j.neuroimage.2011.10.010

Andreasen NC, Endicott J, Spitzer RL, Winokur G (1977) The family history method using diagnostic criteria reliability and validity. Arch Gen Psychiatry 34:1229–1235

Anemüller J, Sejnowski TJ, Makeig S (2003) Complex independent component analysis of frequency-domain electroencephalographic data. Neural Netw 16:1311–1323. doi:10.1016/j.neunet.2003.08.003

Beckmann CF, Smith SM (2005) Tensorial extensions of independent component analysis for multisubject FMRI analysis. Neuroimage 25:294–311

Bell AJ, Sejnowski TJ (1995) An information-maximization approach to blind separation and blind deconvolution. Neural Comput 7:1129–1159

Belouchrani A, Abed-Meraim K, Cardoso J-F, Moulines E (1997) A blind source separation technique using second-order statistics. IEEE Trans Signal Process 45:434–444

Bernat EM, Williams WJ, Gehring WJ (2005) Decomposing ERP time–frequency energy using PCA. Clin Neurophysiol 116:1314–1334. doi:10.1016/j.clinph.2005.01.019

Bridwell DA, Calhoun VD (2014) Fusing concurrent EEG and fMRI intrinsic networks. In: Supek S, Aine C (eds) MEG-from signals to dynamic cortical networks. Springer, Berlin

Bridwell DA, Wu L, Eichele T, Calhoun VD (2013) The spatiospectral characterization of brain networks: fusing concurrent EEG spectra and fMRI maps. NeuroImage 69:101–111

Bridwell DA, Kiehl KA, Pearlson GD, Calhoun VD (2014) Patients with schizophrenia demonstrate reduced cortical sensitivity to auditory oddball regularities. Schizophr Res 158:189–194. doi:10.1016/j.schres.2014.06.037

Bridwell DA, Steele VR, Maurer JM et al (2015) The relationship between somatic and cognitive-affective depression symptoms and error-related ERPs. J Affect Disord 172:89–95. doi:10.1016/j.jad.2014.09.054

Buzsaki G (2006) Rhythms of the brain. Oxford University Press, New York

Calhoun V, Adali T (2012) Multi-subject independent component analysis of fMRI: a decade of intrinsic networks, default mode, and neurodiagnostic discovery. IEEE Rev Biomed Eng 5:60–72

Calhoun VD, Adali T, Pearlson GD, Pekar JJ (2001) A method for making group inferences from functional MRI data using independent component analysis. Hum Brain Mapp 14:140–151

Calhoun VD, Potluru VK, Phlypo R et al (2013) Independent component analysis for brain fMRI does indeed select for maximal independence. PLoS ONE 8:e73309. doi:10.1371/journal.pone.0073309

Cardoso JF, Souloumiac A (1993) Blind beamforming for non-gaussian signals. Radar Signal Process IEE Proc F 140:362–370

Cichocki A, Amari S, Siwek K, Tanaka T (2003) ICALAB Toolboxes

Cong F, He Z, Hämäläinen J et al (2013) Validating rationale of group-level component analysis based on estimating number of sources in EEG through model order selection. J Neurosci Methods 212:165–172. doi:10.1016/j.jneumeth.2012.09.029

Congedo M, Gouy-Pailler C, Jutten C (2008) On the blind source separation of human electroencephalogram by approximate joint diagonalization of second order statistics. Clin Neurophysiol 119:2677–2686. doi:10.1016/j.clinph.2008.09.007

Congedo M, John RE, De Ridder D, Prichep L (2010) Group independent component analysis of resting state EEG in large normative samples. Int J Psychophysiol 78:89–99. doi:10.1016/j.ijpsycho.2010.06.003

Correa N, Adali T, Li Y, Calhoun VD (2005) Comparison of blind source separation algorithms for fMRI using a new MATLAB toolbox: GIFT. In: Proceedings of IEEE International Conference on Acoustics, Speech, Signal Processing (ICASSP). Philadelphia, PA, pp 401–404

Cruces S, Castedo A, Cichochki A (2000) Novel blind source separation algorithms using cumulants. In: Nov Blind Source Sep Algorithms Using Cumulants IEEE International Conference on Acoustics, Speech, and Signal Processing. pp 3152–3155

Cruces S, Cichocki A, Amari S (2001) Criteria for the simultaneous blind extraction of arbitrary groups of sources. In: Proceedings International Conference on ICA and BSS. pp 740–745

Daubechies I (1992) Ten lectures on wavelets. Society for Indistrial and Applied Mathematics, Philadelphia

Delorme A, Makeig S (2004) EEGLAB: an open source toolbox for analysis of single-trial EEG dynamics including independent component analysis. J Neurosci Methods 134:9–21

Delorme A, Palmer J, Onton J et al (2012) Independent EEG sources are dipolar. PLoS ONE 7:e30135

Doron E, Yeredor A (2004) Asymptotically optimal blind separation of parametric Gaussian sources. In: Proceedings of ICA2004. Kyoto, Japan

Eichele T, Calhoun VD, Moosmann M et al (2008) Unmixing concurrent EEG-fMRI with parallel independent component analysis. Int J Psychophysiol 67:222–234

Eichele T, Rachakonda S, Brakedal B et al (2011) EEGIFT: group independent component analysis for event-related EEG data. Comput Intell Neurosci 2011:9

Erhardt EB, Rachakonda S, Bedrick EJ et al (2011) Comparison of multi-subject ICA methods for analysis of fMRI data. Hum Brain Mapp 32:2075–2095. doi:10.1002/hbm.21170

Esposito F, Scarabino T, Hyvarinen A et al (2005) Independent component analysis of fMRI group studies by self-organizing clustering. Neuroimage 25:193–205

Georgiev P, Cichocki A (2001) Blind source separation via symmetric eigenvalue decomposition. In: Sixth International, Symposium on IEEE Signal Processing and its Applications. 2001, pp 17–20

Guo Y, Pagnoni G (2008) A unified framework for group independent component analysis for multi-subject fMRI data. NeuroImage 42:1078–1093

Harmony T (2013) The functional significance of delta oscillations in cognitive processing. Front Integr Neurosci. doi:10.3389/fnint.2013.00083

Himberg J, Hyvärinen A, Esposito F (2004) Validating the independent components of neuroimaging time series via clustering and visualization. Neuroimage 22:1214–1222

Hu L, Zhang ZG, Mouraux A, Iannetti GD (2015) Multiple linear regression to estimate time-frequency electrophysiological responses in single trials. NeuroImage 111:442–453

Huster RJ, Plis SM, Calhoun VD (2015) Group-level component analyses of EEG: validation and evaluation. Front Neurosci. doi:10.3389/fnins.2015.00254

Hyvarinen A, Oja E (1997) A fast fixed-point algorithm for independent component analysis. Neural Comput 9:1483–1492

Hyvarinen A, Karhunen J, Oja E (2001) Independent component analysis. Wiley, New York

Hyvärinen A, Ramkumar P, Parkkonen L, Hari R (2010) Independent component analysis of short-time Fourier transforms for spontaneous EEG/MEG analysis. NeuroImage 49:257–271. doi:10.1016/j.neuroimage.2009.08.028

Kauppi J-P, Parkkonen L, Hari R, Hyvärinen A (2013) Decoding magnetoencephalographic rhythmic activity using spectrospatial information. NeuroImage 83:921–936. doi:10.1016/j.neuroimage.2013.07.026

Klimesch W (1999) EEG alpha and theta oscillations reflect cognitive and memory performance: a review and analysis. Brain Res Rev 29:169–195

Klimesch W, Sauseng P, Hanslmayr S (2007) EEG alpha oscillations: the inhibition–timing hypothesis. Brain Res Rev 53:63–88. doi:10.1016/j.brainresrev.2006.06.003

Kovacevic N, McIntosh AR (2007) Groupwise independent component decomposition of EEG data and partial least square analysis. NeuroImage 35:1103–1112. doi:10.1016/j.neuroimage.2007.01.016

Learned-Miller EG, Fisher JW III (2003) ICA using spacings estimates of entropy. J Mach Learn Res 4:1271–1295

Lee TW, Girolami M, Sejnowski TJ (1999) Independent component analysis using an extended infomax algorithm for mixed subgaussian and supergaussian sources. Neural Comput 11:417–441

Li X-L, Adali T (2010a) Independent component analysis by entropy bound minimization. IEEE Trans Signal Process 58:5151–5164. doi:10.1109/TSP.2010.2055859

Li X-L, Adali T (2010b) Blind spatiotemporal separation of second and/or higher-order correlated sources by entropy rate minimization. In: IEEE International Conference on Acoustics Speech and Signal Processing (ICASSP), 2010. pp 1934–1937

Li Y-O, Adali T, Calhoun VD (2007) Estimating the number of independent components for functional magnetic resonance imaging data. Hum Brain Mapp 28:1251–1266. doi:10.1002/hbm.20359

Lio G, Boulinguez P (2013) Greater robustness of second order statistics than higher order statistics algorithms to distortions of the mixing matrix in blind source separation of human EEG: Implications for single-subject and group analyses. NeuroImage 67:137–152. doi:10.1016/j.neuroimage.2012.11.015

Makeig S, Jung T-P, Bell AJ et al (1997) Blind separation of auditory event-related brain responses into independent components. Proc Natl Acad Sci 94:10979–10984

Makeig S, Debener S, Onton J, Delorme A (2004) Mining event-related brain dynamics. Trends Cogn Sci 8:204–210

Mallat S (2009) A wavelet tour of signal processing, The sparse way, 3rd edn. Elsevier, Amsterdam

Mognon A, Jovicich J, Bruzzone L, Buiatti M (2011) ADJUST: an automatic EEG artifact detector based on the joint use of spatial and temporal features: automatic spatio-temporal EEG artifact detection. Psychophysiology 48:229–240. doi:10.1111/j.1469-8986.2010.01061.x

Nikulin VV, Nolte G, Curio G (2011) A novel method for reliable and fast extraction of neuronal EEG/MEG oscillations on the basis of spatio-spectral decomposition. NeuroImage 55:1528–1535. doi:10.1016/j.neuroimage.2011.01.057

Nolan H, Whelan R, Reilly RB (2010) FASTER: fully automated statistical thresholding for EEG artifact rejection. J Neurosci Methods 192:152–162. doi:10.1016/j.jneumeth.2010.07.015

Nunez P, Srinivasan R (2006) Electric fields of the brain: the neurophysics of EEG, 2nd edn. Oxford University Press, New York

Nyhus E, Curran T (2010) Functional role of gamma and theta oscillations in episodic memory. Neurosci Biobehav Rev 34:1023–1035. doi:10.1016/j.neubiorev.2009.12.014

Onton J, Delorme A, Makeig S (2005) Frontal midline EEG dynamics during working memory. NeuroImage 27:341–356. doi:10.1016/j.neuroimage.2005.04.014

Onton J, Westerfield M, Townsend J, Makeig S (2006) Imaging human EEG dynamics using independent component analysis. Neurosci Biobehav Rev 30:808–822. doi:10.1016/j.neubiorev.2006.06.007

Orekhova EV, Elam M, Orekhov VY (2011) Unraveling superimposed EEG rhythms with multi-dimensional decomposition. J Neurosci Methods 195:47–60. doi:10.1016/j.jneumeth.2010.11.010

Ponomarev VA, Mueller A, Candrian G et al (2014) Group independent component analysis (gICA) and current source density (CSD) in the study of EEG in ADHD adults. Clin Neurophysiol 125:83–97. doi:10.1016/j.clinph.2013.06.015

Porcaro C, Ostwald D, Bagshaw AP (2010) Functional source separation improves the quality of single trial visual evoked potentials recorded during concurrent EEG-fMRI. NeuroImage 1:112–123

Ramkumar P, Parkkonen L, Hari R, Hyvärinen A (2012) Characterization of neuromagnetic brain rhythms over time scales of minutes using spatial independent component analysis. Hum Brain Mapp 33:1648–1662. doi:10.1002/hbm.21303

Ramkumar P, Parkkonen L, Hyvärinen A (2014) Group-level spatial independent component analysis of Fourier envelopes of resting-state MEG data. NeuroImage 86:480–491. doi:10.1016/j.neuroimage.2013.10.032

Schmithorst VJ, Holland SK (2004) Comparison of three methods for generating group statistical inferences from independent component analysis of functional magnetic resonance imaging data. J Magn Reson Imaging 19:365–368

Shou G, Ding L, Dasari D (2012) Probing neural activations from continuous EEG in a real-world task: time-frequency independent component analysis. J Neurosci Methods 209:22–34. doi:10.1016/j.jneumeth.2012.05.022

Stone JV (2004) Independent component analysis: a tutorial introduction. MIT press, Cambridge

Strang G, Nguyen T (1996) Wavelets and filterbanks. Cambridge Press, Cambridge

Tang A (2010) Applications of second order blind identification to high-density EEG-based brain imaging: a review. Adv Neural Netw 2010:368–377

Tang AC, Liu J-Y, Sutherland MT (2005) Recovery of correlated neuronal sources from EEG: the good and bad ways of using SOBI. NeuroImage 28:507–519. doi:10.1016/j.neuroimage.2005.06.062

Tichavsky P, Doron E, Yeredor A, Nielsen J (2006) A computationally affordable implementation of an asymptotically optimal BSS algorithm for AR sources. In: 14th European IEEE Signal Processing Conference, 2006 , pp 1–5

Tichavsky P, Koldovsky Z, Yeredor A et al (2008) A hybrid technique for blind separation of non-gaussian and time-correlated sources using a multicomponent approach. IEEE Trans Neural Netw 19:421–430. doi:10.1109/TNN.2007.908648

Tong L, Liu R, Soon VC, Huang Y-F (1991) Indeterminacy and identifiability of blind identification. Circuits Syst IEEE Trans 38:499–509

Wu L, Eichele T, Calhoun VD (2010) Reactivity of hemodynamic responses and functional connectivity to different states of alpha synchrony: a concurrent EEG-fMRI study. NeuroImage 52:1252–1260

Wu W, Chen Z, Gao S, Brown EN (2011) A hierarchical Bayesian approach for learning sparse spatio-temporal decompositions of multichannel EEG. NeuroImage 56:1929–1945. doi:10.1016/j.neuroimage.2011.03.032

Yeredor A (2000) Blind separation of Gaussian sources via second-order statistics with asymptotically optimal weighting. Signal Process Lett IEEE 7:197–200